

Article ID: 1001-3555(2023)06-0528-07

NiFeOOH Nanosheets Self-supported on the NiFe Alloy Foam for Oxygen Evolution Reaction

WU Mei-xia¹, ZHANG You-fu², YANG Xiao-meng¹, SHANG Jian-peng¹,
GUO Yong¹, LI Zuo-peng^{1*}

(1. School of Chemistry and Chemical Engineering, Shanxi Datong University, Datong 037009, China;

2. Hebei Yanxing Machinery Co., Ltd., Zhangjiakou 075000, China)

Abstract: The electrocatalytic oxygen evolution reaction (OER) is a critical half-cell reaction for hydrogen production *via* water electrolysis. However, the practical OER suffers from sluggish kinetics and thus requires efficient electrocatalyst. Among the non-noble metal catalysts, NiFe-based materials represent one of the most active classes of OER catalysts. In the present work, the self-supporting NiFeOOH catalysts with nanosheet morphology were prepared by oxidation of NiFe alloy foam (NF) *via* a simple one-step impregnation etching method using piranha solution and their OER performances in alkaline were studied in depth. The morphology, structure and composition of electrocatalysts were characterized by SEM, mapping, XRD and XPS, which confirmed the formation of NiFeOOH nanosheet structure on 3D porous substrate. Due to the presence of high-valence Ni, Fe species and the formation of two-dimensional nanosheet structure, the OER performance of NiFeOOH/NF is greatly improved, the overpotential is only 155.68 mV at 10 mA·cm⁻², Tafel slope is only 88.2 mV·dec⁻¹. The results provide a new idea for the development of efficient and durable self-supporting non-noble metal electrode.

Key words: NiFeOOH nanosheets; piranha solution; self-supported; oxygen evolution reaction

CLC number: O643.32

Document code: A

DOI: 10.16084/j.issn1001-3555.2023.06.002

With the proposed emission peaks and carbon neutrality goals, renewable energy power generation driven water cracking hydrogen production technology is developing at an unprecedented speed. On the one hand, it can reduce the waste of wind power and photovoltaic energy, thereby promoting the maximum utilization of wind and solar energy; On the other hand, as an efficient and environmentally friendly technology, it is very suitable for the goal of sustainable development. However, the slow oxygen evolution reaction (OER) in electrolytic water severely limits the large-scale application of this technology. Therefore, more and more electrocatalysts have been studied to accelerate OER.

Among the non-noble metal electrocatalysts developed for OER, NiFe based materials have attracted considerable attention due to their abundant reserves and excellent performance under alkaline conditions. As early as the last century, Corrigan^[1-2] conducted a series of studies on iron doped nickel hydroxide, and other research groups further studied^[3-6]. The results showed that appropriate iron doping can improve the valence of nickel and form more active sites. It is well known that NiFe oxyhydroxide has excellent activity for OER. Fan^[7] synthesized NiFeOOH with abundant oxygen vacancies (O_v). The results showed that the shortened Fe—O bonds and oxygen defects of NiFeOOH synergistically

improved the interaction between the metal cations and intermediate species, which was beneficial to accelerating the entire reaction kinetics. A three-dimensional integrated anode electrode was prepared by electrodeposition of NiFeOOH on a gas diffusion layer instead of conventional electrode, which has stable activity over 500 h^[8]. In addition, comparing the reported literatures^[9-17], it can also be found that different nanostructured materials have different catalytic properties. Rong et al.^[18] reported a series of NiFeOOH materials for OER. When the Ni/Fe molar ratio is 7, the morphology of NiFeOOH remains nanoflakes, but when the Ni/Fe molar ratio is further reduced, it transfers from nanoflakes to bulk particles. Accordingly, their performance varies. Due to their unique two-dimensional (2D) structure, nanosheets have a large plane size while maintaining atomic thickness, so they have a large specific surface area; and the high exposure of surface atoms provides conditions for easy control of material properties through surface modification/functionalization, elemental doping or defects, strain, phase engineering, etc^[19]. Therefore, it is of great significance to prepare NiFeOOH catalyst with nanosheet morphology. Up to now, the conventional methods for preparing these catalysts mainly include hydrothermal/solvothermal, co-precipitation and electrolytic deposition. However, all of these methods require additional device and energy supplementation, which are costly

Received date: 2023-07-31; **Revised date:** 2023-10-09.

Foundation: Natural Science Foundation of Shanxi (201901D111310, 201801D221057); Postgraduate Educational reform and research program in Shanxi province(2022YJJG255) and Natural Science Foundation of Shanxi Datong University(2022K23).

Biography: Wu Mei-xia (1977–), female, doctor, associate professor, mainly engaged in research of water splitting for hydrogen production driven by clean energy.

* Corresponding authors. E-mail: lizuopeng@126.com.

and run counter to green energy. So it is necessary to develop new cost-effective strategies to synthesize efficient nickel-iron-based materials. In addition, transition metal-based electrocatalysts are usually combined with polymer binders such as Nafion as electrodes, resulting in poor electrical conductivity and mechanical stability. A feasible solution is to directly grow active electrocatalysts on conductive substrates such as nickel foam electrode plates.

From a chemical perspective, corrosion products often form compounds of metal (hydro) oxides and may contain sulfides or chlorides, which can be used as a general method for producing unconventional nanostructures^[20]. Inspired by the above discussion, a new OER electrocatalyst was synthesized in this work. NiFeOOH nanosheets were grown on the surface of NF by controlling the corrosion conditions. Interestingly, the synergistic effect of Ni and Fe is significantly beneficial to the formation of -OOH. At the same time, as a conductive substrate, NF can not only obtain a three-dimensional structure with large surface area, but also simplify the preparation process without adding additional Ni, Fe element.

1 Experimental

1.1 Preparation of catalysts

NF with different Fe content was prepared according to our previous report^[21]. NiFe alloy was electrodeposited on the treated polyurethane sponge by constant current electrolysis. The ratio of Ni to Fe in the NiFe alloy can be adjusted according to the mass changes of $\text{FeSO}_4 \cdot 7\text{H}_2\text{O}$ and $\text{NiSO}_4 \cdot 6\text{H}_2\text{O}$. After 1~2 h of plating, a shiny metallic porous NiFe alloy was obtained. Piranha solution (PS) is a mixture of sulfuric acid (H_2SO_4 , 95%~98%, Tianjin Chemical Reagent) and hydrogen peroxide (H_2O_2 , 30% (Mass fraction) in H_2O , Tianjin Chemical Reagent) (3 : 1 by volume ratio) and left to cool completely. NF was soaked in the PS at a controlled temperature for different periods of time, then taken it out and cleaned by deionized water and ethanol for three times, respectively. Finally, the sample was dried in a vacuum drying oven at 40 °C, marked as NiFe-PS. Additionally, the samples prepared by varying only the reaction medium (H_2SO_4 or H_2O_2) were labeled as NiFe- H_2SO_4 and NiFe- H_2O_2 under otherwise identical conditions.

1.2 Catalyst characterization

X-ray powder diffraction (XRD) was performed using a Rigaku Smartlab SE X-ray diffractometer with $\text{Cu K}\alpha$ radiation ($\lambda = 0.15418 \text{ nm}$) at a scanning rate of $2^\circ \cdot \text{min}^{-1}$ in the 2θ range of $5^\circ \sim 80^\circ$. The morphology and elemental mapping of the prepared samples were observed by scanning electron microscopy (SEM) (TESCAN MAIA 3 LMH) coupled with elemental Mapping. The compositions of the as-prepared samples were analyzed by inductively coupled plasma analysis (ICP Varrian 720). The elemental valences were analyzed by X-ray photoelectron spectroscopy (XPS) with a ESCALAB 250xi using a monochromatic $\text{Al K}\alpha$ X-ray beam (1486.6 eV).

1.3 Electrochemical measurements

The catalytic performance was measured on a CHI760E electrochemical workstation (CH Instruments, Inc., Shanghai) in a standard three-electrode system, the Self-supported catalyst ($0.5 \text{ cm} \times 0.5 \text{ cm}$) as working electrode, a Pt foil electrode ($1.0 \text{ cm} \times 1.5 \text{ cm}$) and an Ag/AgCl electrode were served as the counter and reference electrode, respectively. In all analysis, the Ag/AgCl reference electrode was calibrated with respect to

reversible hydrogen electrode (RHE) according to $E(\text{RHE}) = E(\text{Ag}/\text{AgCl}) + 0.204 + 0.059 \text{ pH}$ in $1.0 \text{ mol} \cdot \text{L}^{-1}$ KOH. The overpotential (η) was calculated by $E(\text{RHE}) - 1.23 \text{ V}$. Linear sweep voltammetry (LSV) measurements were conducted in the electrolyte at scan rate of $5 \text{ mV} \cdot \text{s}^{-1}$ (scanning range from 0 to 1.5 V). Chronopotential curve was recorded to evaluate the lifetime of electrocatalyst for OER. Electrochemical impedance spectroscopy (EIS) measurements were performed on Zahner electrochemical workstation (Cimpes-2, Germany) by applying an AC voltage of 10 mV amplitude in a frequency range from 0.01 Hz to 100 kHz at 1.623 V.

2 Results and discussion

The XRD patterns of the samples are shown in Fig. 1. NF shows three obvious and sharp peaks, which are well matched with the phase of Ni_3Fe alloy (PDF 38-0419). For NiFe-PS, it can be clearly observed that there is also an obviously wide peak at around 21° , which may be assigned to the NiFeOOH^[22-23] besides the corresponding peak of NF. However, the intensity of NiFeOOH is very weak, possibly due to the poor crystallinity of NiFe alloy covered with a very thin catalyst film. In addition, there are two tiny peaks at 21.7° and 31.1° respectively, indicating the presence of S^[24]. Interestingly, these other peaks were not observed in the samples treated with H_2O_2 or H_2SO_4 alone, suggesting that the catalytic performance of samples may differ under different oxidation conditions.

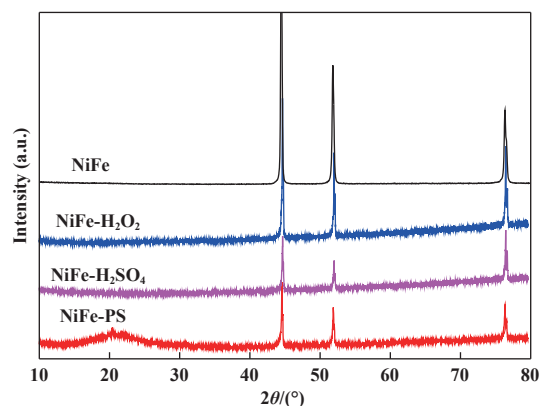


Fig.1 The XRD patterns of catalysts at different oxidation conditions

The morphology of 10%NiFe alloy before and after oxidation was analyzed by SEM, as shown in Fig. 2. The surface of the sample has undergone significant changes. Significant surface changes can be observed after oxidation of the sample. Comparing Fig. 2 ((a), (b), (c)) and Fig. 2 ((d), (e), (f)), it was found that the surface of the unoxidized NiFe alloy was relatively smooth and clean. After oxidation, the surface became significantly rougher, and nanosheet morphology was grown, with a thickness of about 25 nm. In addition, as shown in Fig. 2(f), at low magnification, the nanosheets generated on the surface have a nearly spherical structure, forming an interconnected network structure with open pores overall, which is similar to the morphology of NiFeOOH prepared by hydrothermal method in references^[24-25]. This structure may provide a larger accessible area of electrolyte and more mass/ion diffusion pathways, therefore promote OER kinetics to obtain better activity. Fig. 2((g)-(k)) shows the elemental spectrum of NiFeOOH/NF, identifying four elements, namely Ni, Fe, S, and O. Among these elements, the distribution of O

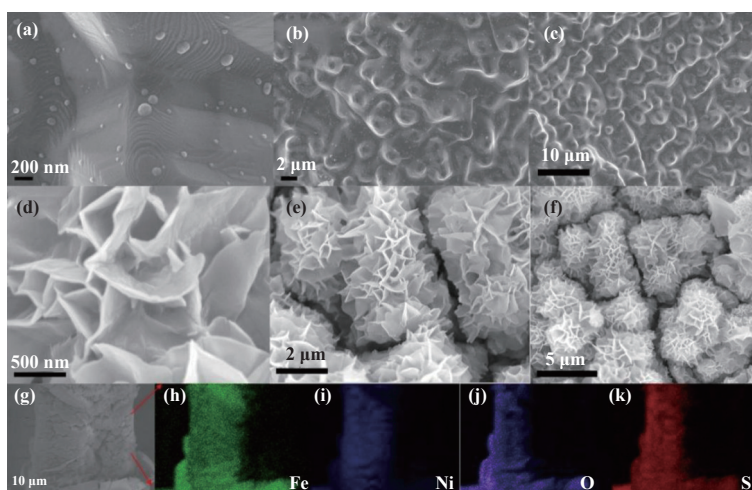


Fig.2 The SEM images of 10%NiFe alloy foam before ((a), (b), (c)) and after ((d), (e), (f)) oxidation and mapping ((g)–(k))

element is significantly expanded compared to NiFe alloy, indicating that the surface of NF is oxidized. The uniform distribution of S not only indicates that the piranha solution did indeed oxidize the NiFe alloy during the preparation process, but also suggests that the OER performance of the catalyst may be affected by S element.

Also, as shown in Fig. 3, the morphology of foamed NiFe alloys with different Fe contents (10%, 20%, 30% and 50%)

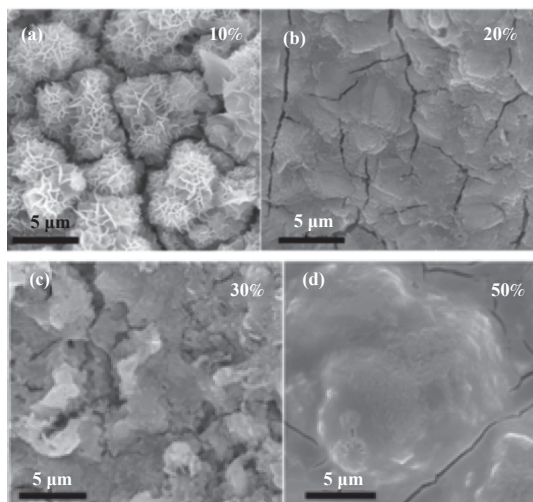


Fig.3 The SEM images of NiFeOOH/NF with different Fe contents(10%(a), 20%(b), 30%(c), 50%(d))

after oxidation was further characterized by SEM. In contrast, NF with Fe content of 10% presented with the shape of nanosheets after oxidation, while other samples with different Fe content only become rougher, forming irregular and large-sized agglomerations, which differed significantly from the morphology of 10%NiFe-PS. The results indicate that the OER performance of oxidized samples with different iron contents may vary. Inductively coupled plasma (ICP) analysis was used to confirm the component contents in the as-prepared NF with different Fe contents. The Fe and Ni contents by weigh in NF samples with different Fe contents (10%, 20%, 30% and 50%) are 9.12%, 88.90%; 17.47%, 80.94%; 28.08%, 69.42% and 48.55%, 50.38%, respectively.

In order to further determine the composition and valence states of the catalyst by XPS test. The Fig. 4(a) shows the high-resolution XPS of Ni $2p$ of the samples. For NF, there are four obvious spin-orbit peaks of Ni $2p_{3/2}$ and $2p_{1/2}$ at 852.36/855.65 and 869.54/873.45 eV, respectively, the former two peaks can be unambiguously identified as the metallic Ni and the latter two can be assigned to the Ni²⁺, the other peaks with the binding energies at 861.35 and 879.13 eV are the corresponding satellite peaks, this is typical peak of Ni²⁺[26]. Furthermore, according to the pertinent literatures, the binding energy difference is 17.8 eV between the $2p_{1/2}$ and $2p_{3/2}$, suggesting that the existence of Ni(OH)₂ in the catalyst[27], by contrast, for NiFe-PS, metallic Ni peak intensity decreases drastically, the shift to slightly higher binding energy (~0.7 eV) means that a change in the electronic structure occurs upon the phase conversion. Therefore, the peaks of 856.35 and 874.25 eV are assigned to Ni³⁺[28–30]. Significantly, there is a new weak peak at 858.31 eV which can be ascribed to Ni⁴⁺[31]. The Fe $2p$ is shown in Fig. 4(b), for the NiFe-PS, the peaks of 711.35 and 724.28 eV are assigned to $2p_{3/2}$ and $2p_{1/2}$ of Fe³⁺[27], the peak of 705.48 eV belong to metallic Fe³⁺, and the former is stronger than NF, while the latter is lower than it, indicating that PS accelerated the oxidation of Fe. The O $1s$ spectrum is shown in Fig. 4(c), it exhibits three peaks located at 529.73, 531.73 and 533.22 eV, which are successively ascribed to the M—O bonds, M—OH bonds and absorbed H₂O[27, 31]. Compared with NF, the peak intensity of M—OH is stronger, indicating the content of NiFeOOH is higher, and in NF, the peak of 529.22 eV is ascribed to Ni—O bonds, indicating that PS tend to promote the formation of M—OH bonds and Fe—O bonds. All the above results demonstrate that PS accelerates the oxidation of NF and the formation of NiFeOOH. In the S $2p$ spectrum (Fig. 4(d)), the presence of S is completely negligible in NF, while for the NiFe-PS, there are obvious two peaks located in 168.7 and 169.98 eV, which correspond to residual sulfate groups or oxidized sulfur species due to surface oxidation[32], the results show that the surface of the oxidized catalyst contains S element that can reduce the adsorption free energy of OH^{*} and the free energy between O^{*} and OH^{*}[33], thereby improving OER performance.

The electrochemical performance of NF at different oxidation condition was tested. As is shown in Fig. 5((a), (b)),

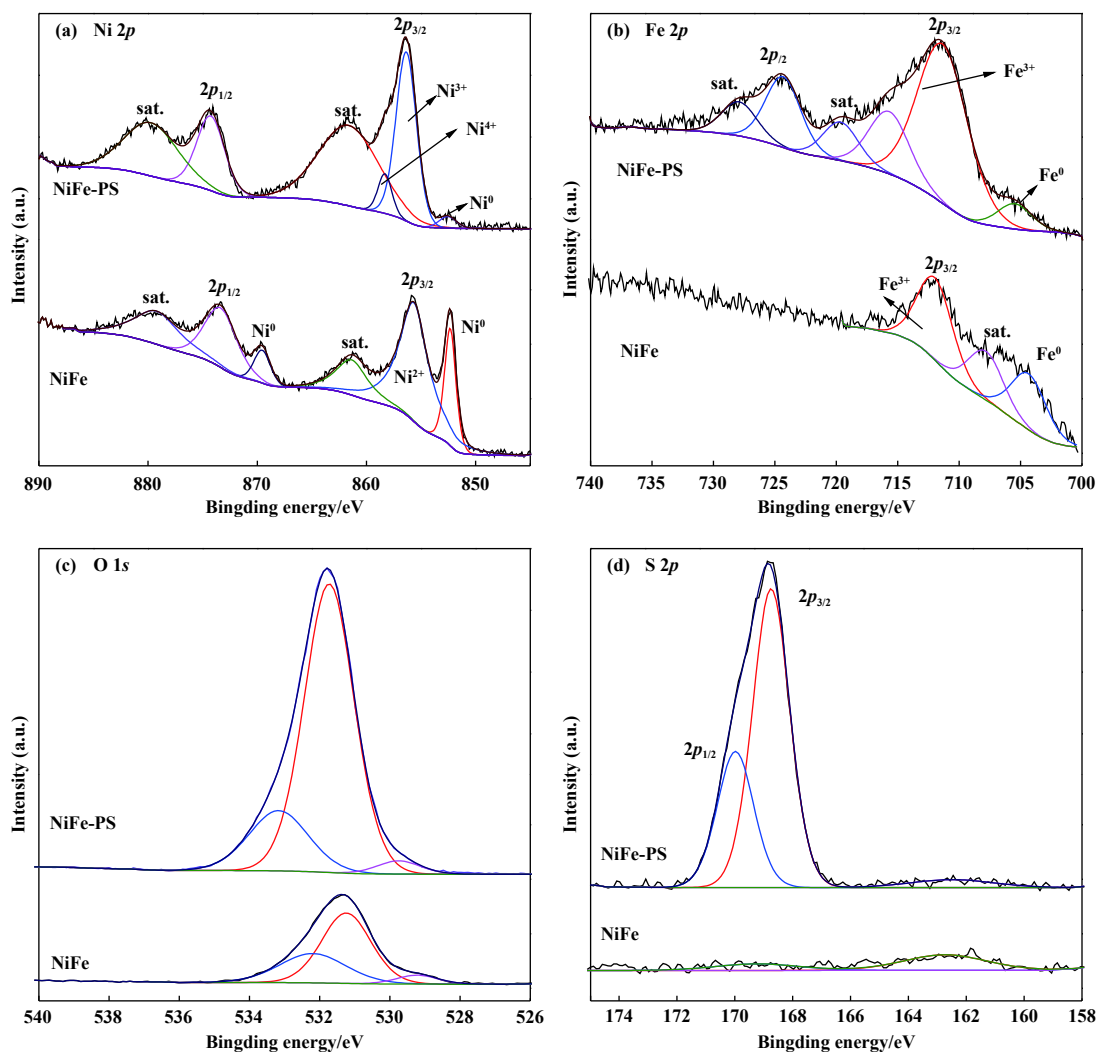


Fig.4 XPS spectra of NiFe-PS and NiFe: Ni 2p(a); Fe 2p(b); O 1s(c); S 2p(d)

the overpotentials of NiFeOOH/NF at 30, 50, 80 and 120 °C were 215.11, 217.87, 174.26 and 155.68 mV at $10 \text{ mA}\cdot\text{cm}^{-2}$, respectively, the Tafel slopes were 182, 271.8, 92.7 and 50.8 $\text{mV}\cdot\text{dec}^{-1}$, respectively, which were consistent with the overpotential results. When the oxidation at higher temperature than 120 °C, it is found that the NF very quickly dissolved in PS solution. Therefore, the sample prepared at 120 °C has the lowest overpotential and Tafel slope, showing reaction kinetics of the catalyst is the fastest, indicating that the oxidation of the catalyst would be promoted with increasing of the temperature, so catalytic performance is increased. Then, the influence of different oxidation time on samples was studied, as shown in Fig. 5(c), (d). At $10 \text{ mA}\cdot\text{cm}^{-2}$, the overpotentials of samples were 201.53, 155.68, 176.85 and 167.09 mV at 5, 10, 20 and 30 min, respectively, and their Tafel slopes were 170.9, 64.6, 71.8 and 81.8 $\text{mV}\cdot\text{dec}^{-1}$, respectively. The results of overpotential and Tafel slope show that the overpotential increases firstly and then decreases with the increase of oxidation time, which may be attributed the number of $\text{Ni}^{3+}/\text{Ni}^{4+}$ and Fe^{3+} on the surface of samples were increased with the increase of oxidation time. Surface formation of α -FeOOH may block the active site of NiFe hydroxyl oxide if the oxidation time for too long, thereby reducing its availability^[34].

The influence of catalysts with different Fe content on OER performance was investigated. Fig. 5(e) showed the LSV curves of different samples. Compared with NF with 30% Fe content, other samples oxidized by PS showed no oxidation peak between 0.2~0.3 V. Combined with XPS analysis, it was speculated that this might be due to the strong oxidation of PS, so the state of Ni was directly oxidized to +3 during the preparation process. The overpotentials of 10%NiFe-PS, 20%NiFe-PS, 30%NiFe-PS and 50%NiFe-PS were 155.68, 189.14, 179.24 and 186.39 mV at $10 \text{ mA}\cdot\text{cm}^{-2}$, respectively. As can be seen from Fig. 5(a), the overpotentials of NiFe-PS are significantly lower than that of NF (293.74 mV). Among NiFe-PSs with different Fe content, 10%NiFe-PS has the smallest overpotential. Further analysis was conducted on the Tafel slope of the sample. As shown in Fig. 5(f), the values were 88.2, 147.6, 98, 111.2 and 120.3 $\text{mV}\cdot\text{dec}^{-1}$, respectively. The Tafel slope of the other samples was lower than that of the untreated samples except for 20%NiFe-PS, and the Tafel slope of 10%NiFe-PS is the lowest. The results showed that the OER performance and reaction kinetics of 10%NiFe-PS were excellent, and the OER performance of the catalyst was affected by the content of Fe element, suggesting that in addition to Ni, Fe may also be the catalytic active site in the

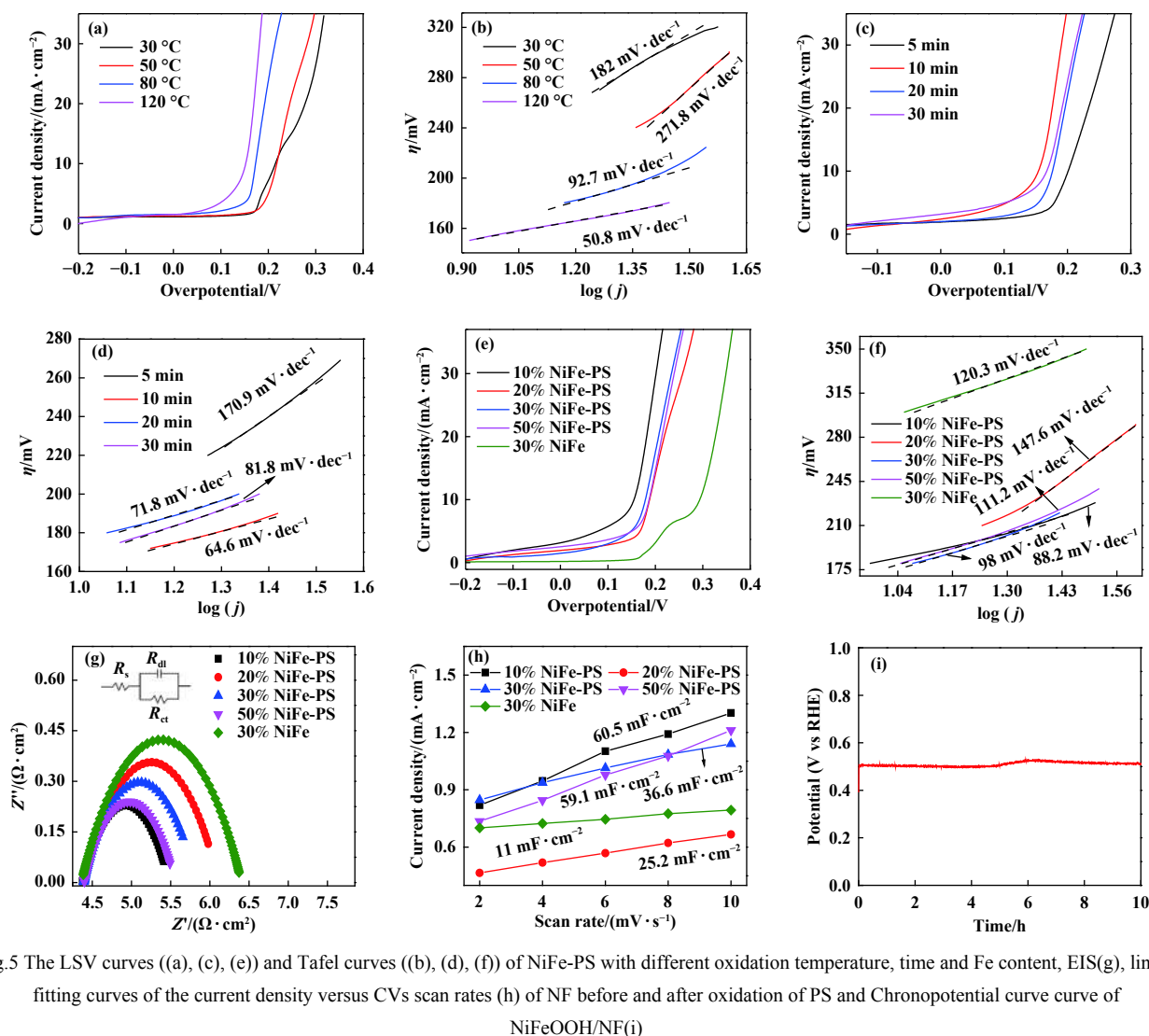


Fig. 5 The LSV curves ((a), (c), (e)) and Tafel curves ((b), (d), (f)) of NiFe-PS with different oxidation temperature, time and Fe content, EIS(g), linear fitting curves of the current density versus CVs scan rates (h) of NF before and after oxidation of PS and Chronopotential curve curve of NiFeOOH/NF(i)

reaction process.

High conductivity is important for the enhancement of catalytic performance. To further investigate the speed of catalytic reaction kinetics, electrochemical impedance spectroscopy (EIS) was used to measure the charge transfer resistance at the reaction interface between the catalyst and the solution. The semicircle in the figure corresponds to the charge transfer resistance (R_{ct}), which is related to electrocatalytic kinetics. The smaller the R_{ct} , the faster the reaction rate, which is conducive to efficient charge transfer. Compared with other samples, the semicircle radius of 10%NiFe-PS is the smallest (Fig. 5(g)), indicating that it has the lowest R_{ct} ($1.159 \Omega \cdot \text{cm}^2$) and the fastest charge transfer rate, which not only confirms the effect of PS on samples, but also indicates that S-doped NiFeOOH nanosheets optimize the electronic structure and accelerates the electron transfer, which is consistent with the above results. In order to further understand the intrinsic activity of catalysts, the CV curves of the catalyst at different sweep speeds in the nonfaraday region were tested and the fitting curves of the current density and scanning rate were obtained to characterize the electrical double-layer capacitor (C_{dl}), so as to further compare the corresponding large electrochemically active surface area (ECSA). It has been

reported that ECSA is generally proportional to the C_{dl} of electrocatalysts. The higher the ECSA value, the better the electrocatalytic activity. As is shown in Fig. 5(h), the slope of 10%NiFe-PS is the largest, and the slope of NF is the smallest, indicating that the ECSA of NiFeOOH/NF increases, which further verifies the LSV results and is consistent with the SEM results.

In addition, the stability of catalysts is an important criterion for evaluating the performance and wide application of electrocatalysts. The potential change of NiFeOOH/NF in 1M NaOH at $10 \text{ mA} \cdot \text{cm}^{-2}$ was studied, as shown in Fig. 5(i). The potential of NiFeOOH/NF catalyst initially increased, remained unchanged for 5 h, then increased slightly by 30 mV, and then decreased slightly after 6 h. During the entire test process, significant changes in the potential occurred at the initial stage, but could be ignored at the later stage. The potential remained stable at 300 mV, indicating that NiFeOOH/NF has good long-term stability. The above data indicates that the as-prepared NiFeOOH/NF catalyst is an efficient catalyst for OER in terms of both catalytic activity and stability. The remarkable OER performance of NiFeOOH/NF can be attributed to the following factors: on the one hand, NF has high electrical conductivity, which is conducive to electron transfer between the active

NiFeOOH and the Ni substrate, and the porous NF provides larger specific surface area and active catalytic sites. On the other hand, NiFeOOH has inherently excellent OER performance, and *in-situ* grown NiFeOOH is conducive to electron transfer between the substrate and the active species, exposing more active sites.

3 Conclusions

In conclusion, the self-supported NiFeOOH/NF electrocatalyst was prepared by *in-situ* growth of NiFeOOH nanosheets on the surface of NF oxidized in piranha solution *via* impregnation etching method. NiFeOOH/NF exhibit excellent OER electrocatalytic activity under alkaline conditions. In 1 mol·L⁻¹ NaOH solution, the current density of 10 mA·cm⁻² only needs 171.96 mV over potential. On basis of these, the excellent OER performance of the catalyst may be attributed to: (1) A synergistic effect between NiFeOOH and NiFe alloy; (2) The existence of high-valence state (Ni³⁺/Ni⁴⁺/Fe³⁺) in 10%NiFe-PS; (3) The formation of nanosheets can increase the electroactive area of the catalyst, thereby enhancing its electrocatalytic performance. As a joint result of above advantages, the OER performance of NiFeOOH/NF was improved.

References

- Corrigan D A, Conell R S. In situ mossbauer study of redox processes in a composite hydroxide of iron and nickel[J]. *J Phys Chem C*, 1987, **91**: 5009–5011.
- Corrigan D A. The catalysis of the oxygen evolution reaction by iron impurities in thin film nickel oxide electrodes[J]. *J Electrochem Soc*, 1987, **134**: 377–384.
- Li Q, He T, Jiang X, *et al.* Boosting oxygen evolution activity of nickel iron hydroxide by iron hydroxide colloidal particles[J]. *J Colloid Interface Sci*, 2022, **606**: 518–525.
- Wang Y, Tao S, Lin H, *et al.* Atomically targeting NiFe LDH to create multivacancies for OER catalysis with a small organic anchor[J]. *Nano Energy*, 2021, **81**: 105606.
- Trotochaud L, Young S L, Ranney J K, *et al.* Nickel-iron oxyhydroxide oxygen-evolution electrocatalysts: the role of intentional and incidental iron incorporation[J]. *J Am Chem Soc*, 2014, **136**: 6744–6753.
- Li N, Bediako D K, Hadt R G, *et al.* Influence of iron doping on tetravalent nickel content in catalytic oxygen evolving films[J]. *Proc Natl Acad Sci USA*, 2017, **114**: 1486–1491.
- Dong J, Wang Y, Jiang Q, *et al.* Charged droplet-driven fast formation of nickel-iron (oxy)hydroxides with rich oxygen defects for boosting overall water splitting[J]. *J Mater Chem A*, 2021, **9**: 20058–20067.
- Park J E, Park S, Kim M J, *et al.* Three-dimensional unified electrode design using a NiFeOOH catalyst for superior performance and durable anion-exchange membrane water electrolyzers[J]. *ACS Catal*, 2021, **12**: 135–145.
- Wu Q, Li T, Wang W, *et al.* High-throughput chainmail catalyst FeCo@C nanoparticle for oxygen evolution reaction[J]. *Int J Hydrogen Energy*, 2020, **45**: 26574–26582.
- Xiang D, Bo X, Gao X, *et al.* Novel one-step synthesis of core@shell iron-nickel alloy nanoparticles coated by carbon layers for efficient oxygen evolution reaction electrocatalysis[J]. *J Power Sources*, 2019, **438**: 226988.
- Chen J S, Ren J, Shalom M, *et al.* Stainless steel mesh-supported NiS nanosheet array as highly efficient catalyst for oxygen evolution reaction[J]. *ACS Appl Mater Interfaces*, 2016, **8**: 5509–5516.
- Masa J, Weide P, Peeters D, *et al.* Amorphous cobalt boride (Co₂B) as a highly efficient nonprecious catalyst for electrochemical water splitting: Oxygen and hydrogen evolution[J]. *Adv Energy Mater*, 2016, **6**: 1502313.
- Choi J, Kim D, Zheng W, *et al.* Interface engineered NiFe₂O₄/NiMoO₄ nanowire arrays for electrochemical oxygen evolution[J]. *Appl Catal B: Environ*, 2021, **286**: 119857.
- Li M, Tao L, Xiao X, *et al.* Core-shell structured NiCo₂O₄@FeOOH nanowire arrays as bifunctional electrocatalysts for efficient overall water splitting[J]. *ChemCatChem*, 2018, **10**: 4119–4125.
- Chang J, Xiao Y, Xiao M, *et al.* Surface oxidized cobalt-phosphide nanorods as an advanced oxygen evolution catalyst in alkaline solution[J]. *ACS Catal*, 2015, **5**: 6874–6878.
- Wang H, Wang J, Pi Y, *et al.* Double perovskite LaFe_xNi_{1-x}O₃ nanorods enable efficient oxygen evolution electrocatalysis[J]. *Angew Chem Int Ed*, 2019, **58**: 2316–2320.
- Li Y, Tong R, Zhang W, *et al.* Pre-intercalation of phosphate into Ni(OH)₂/NiOOH for efficient and stable electrocatalytic oxygen evolution reaction[J]. *J Catal*, 2022, **410**: 22–30.
- Rong F, Zhao J, Yang Q, *et al.* Nanostructured hybrid NiFeOOH/CNT electrocatalysts for oxygen evolution reaction with low overpotential[J]. *RSC Adv*, 2016, **6**: 74536–74544.
- Liu C, Han Y, Yao L, *et al.* Engineering bimetallic NiFe-based hydroxides/selenides heterostructure nanosheet arrays for highly-efficient oxygen evolution reaction[J]. *Small*, 2021, **17**: 2007334.
- Liu H, Fu C, Gu T, *et al.* Corrosion behavior of carbon steel in the presence of sulfate reducing bacteria and iron oxidizing bacteria cultured in oilfield produced water[J]. *Corros Sci*, 2015, **100**: 484–495.
- Yang X, Li Z, Qin J, *et al.* Preparation of Ni-Fe alloy foam for oxygen evolution reaction[J]. *J Fuel Chem Technol*, 2021, **49**(6): 827–834.
- Shin C H, Wei Y, Park G, *et al.* High performance binder-free Fe–Ni hydroxides on nickel foam prepared in piranha solution for the oxygen evolution reaction[J]. *Sustain Energy Fuels*, 2020, **4**: 6311–6320.
- Zhao B, Zhang B, Lu C, *et al.* Hierarchical hollow nanocages of Ni-Co amorphous double hydroxides for high-performance asymmetric supercapacitors[J]. *J Alloys Compd*, 2020, **833**: 155130.
- Li J, Song J, Huang B Y, *et al.* Enhancing the oxygen evolution reaction performance of NiFeOOH electrocatalyst for Zn-air battery by N-doping[J]. *J Catal*, 2020, **389**: 375–381.
- Tian J, Zhang A, Liu R, *et al.* Preparation of CoS₂ supported flower-like NiFe layered double hydroxides nanospheres for high-performance supercapacitors[J]. *J Colloid Interface Sci*, 2020, **579**: 607–618.
- Panda C, Menezes P W, Yao S, *et al.* Boosting electrocatalytic hydrogen evolution activity with a NiPt₃@NiS heteronanostructure evolved from a molecular nickel-platinum precursor[J]. *J Am Chem Soc*, 2019, **141**: 13306–13310.
- Hu H S, Si S, Liu R J, *et al.* Iron-nickel hydroxide nanoflake arrays supported on nickel foam with dramatic catalytic properties for the evolution of oxygen at high current densities[J]. *Int J Energy Res*, 2020, **44**: 9222–9232.
- Liang H, Gandi A N, Xia C, *et al.* Amorphous NiFe-OH/NiFeP electrocatalyst fabricated at low temperature for water oxidation applications[J]. *ACS Energy Lett*, 2017, **2**: 1035–1042.
- Wu Z, Zou Z, Huang J, *et al.* NiFe₂O₄ nanoparticles/NiFe layered double-hydroxide nanosheet heterostructure array for efficient overall water splitting at large current densities[J]. *ACS Appl Mater Interfaces*, 2018, **10**: 26283–26292.
- Liu J, Ding P, Zhu Z, *et al.* Engineering self-reconstruction *via* flexible components in layered double hydroxides for superior-evolving performance[J]. *Small*, 2021, **17**: 2101671.
- Hu F, Wang H, Zhang Y, *et al.* Designing highly efficient and long-term durable electrocatalyst for oxygen evolution by coupling B and P into amorphous porous NiFe-based material[J]. *Small*, 2019, **15**: 1901020.
- Yang Y, Yao H, Yu Z, *et al.* Hierarchical nanoassembly of MoS₂/Co₉S₈/Ni₃S₂/Ni as a highly efficient electrocatalyst for overall water splitting in a wide pH range[J]. *J Am Chem Soc*, 2019, **141**: 10417–10430.
- Li B, Jian J, Chen J, *et al.* Nanoporous 6H-SiC photoanodes with a conformal coating of Ni-FeOOH nanorods for zero-onset-potential water splitting[J]. *ACS Appl Mater Interfaces*, 2020, **12**: 7038–7046.
- Zhao W, Xu H, Luan H, *et al.* NiFe layered double hydroxides grown on a corrosion-cell cathode for oxygen evolution electrocatalysis[J]. *Adv Energy Mater*, 2021, **12**: 2102372.

泡沫镍铁合金自支撑 NiFeOOH 纳米片的制备及析氧性能研究

武美霞¹, 张有富², 杨肖萌¹, 尚建鹏¹, 郭 永¹, 李作鹏^{1*}

(1. 山西大同大学 化学与化工学院, 山西 大同 037009; 2. 河北燕兴机械有限公司, 河北 张家口 075000)

摘要: 电催化析氧反应 (OER) 是电解水制氢的重要半电池反应. 然而, OER 的缓慢动力学仍需研究高效的电催化剂. 在非贵金属催化剂中, NiFe 基材料是 OER 催化剂研究热点. 我们通过食人鱼溶液简单一步浸渍刻蚀法将不同 Fe 含量的泡沫 NiFe 合金进行氧化, 制备了表面具有纳米片形貌的 NiFeOOH 自支撑电催化剂, 并深入研究其电催化析氧性能. 通过 SEM、XRD、XPS 等对电催化剂的形貌结构及成分进行表征, 证实了三维多孔基底上 NiFeOOH 纳米片结构的形成. 由于高价镍、铁物种的存在以及二维纳米片结构的生成, NiFeOOH/NF 的析氧性能大幅度提高, 在 $10 \text{ mA}\cdot\text{cm}^{-2}$ 的电流密度下过电位仅 155.68 mV, Tafel 斜率为 $88.2 \text{ mV}\cdot\text{dec}^{-1}$. 这为研制高效、耐用的自支撑非贵金属电极提供了新思路.

关键词: NiFeOOH 纳米片; 食人鱼溶液; 自支撑; 析氧反应

关于《分子催化》文种变更为中英文的公告

经国家新闻出版署 (国新出审 [2023]1712 号文件) 批准, 《分子催化》文种由中文变更为中英文, 国内统一连续出版物号由 CN62-1039/O6 变更为 CN62-1227/O6, 《期刊出版许可证》期刊名称登记为《分子催化 (中英文)》。自批准之日 (2023 年 10 月 17 日) 起, 本刊将接受中英文稿件投稿。中文稿件要求附英文题目、作者及单位、英文详细摘要及关键词, 英文稿件要求附中文题目、作者及单位、中文详细摘要及关键词。欢迎大家登录《分子催化 (中英文)》期刊网站踊跃投送中英文稿件, 关注分子催化微信公众号及时了解期刊动态信息。

感谢各级领导、专家学者、作者、读者及相关单位长期以来给予本刊的支持和厚爱!

《分子催化 (中英文)》编辑部

2023 年 12 月 1 日